Attosecond cascades and time delays in one-electron photoionization

Suren Sukiasyan,[1] Kenichi L. Ishikawa,[2] and Misha Ivanov[1,3]
[1]*Department of Physics, Imperial College London, South Kensington Campus, SW7 2AZ London, United Kingdom*
[2]*Photon Science Center, Graduate School of Engineering, The University of Tokyo, 7-3-1 Hongo, Bunkyo-ku, Tokyo 113-8656, Japan*
[3]*Max Born Institute, Max Born Strasse 2a, D-12489 Berlin Adlershof, Berlin Germany*
(Received 1 November 2011; published 21 September 2012)

We present time-resolved *ab initio* study of the attosecond dynamics of electron-electron correlation during single-electron, single XUV-photon ionization of an excited helium atom. We identify multiple time scales in these dynamics, caused by the interplay of the initial shake-up excitation with the excitation cascades induced by the postionization interaction of the outgoing electron with the core. The time scales and the structure of these excitation cascades are directly linked to the time it takes the "active" continuum electron, lifted from a deeper bound orbital, to traverse the orbit of the "passive" electron residing in the outer orbit.

DOI: 10.1103/PhysRevA.86.033423 PACS number(s): 32.80.Fb, 32.80.Rm, 42.50.Hz

Experiments on time-resolving photoionization dynamics have now reached the level of few tens to few attoseconds [1–4], putting attosecond-resolved analysis of electron-electron correlations firmly within reach. First experiments brought first surprises, indicating long apparent time delays [3,4] in photoionization, inconsistent with predictions of theoretical calculations [3,5]. Possible causes for the discrepancy have been scrutinized theoretically [3–10], including the effect of the measurements, which relied on using the so-called attosecond streak camera [11,12] or the reconstruction of attosecond beating by interference of two-photon transitions (RABBIT) [13] techniques. While even the most complete simulations to date [10] are still about a factor of 2 short of the experiments [3], these studies have brought to the focus rich correlation-driven dynamics that contribute to photoionization delays [5,10,14–16].

Our goal is to directly visualize and analyze these correlation-driven dynamics using a simpler benchmark system, helium, and an even simpler model system. In both cases, we setup the initial conditions such that correlation-driven dynamics is brought to the fore. The relative simplicity of *ab initio* calculations in these systems, compared to the *tour de force* calculations for neon [10], allows for a detailed analysis of the underlying physics. We present the full treatment of the excited He atom and results for a one-dimensional (1D) two-electron model. In the latter case, electrons are restricted to a single degree of freedom each, and the electron-electron and electron-nucleus Coulomb interactions are softened (the two-electron model atom introduced by Eberly and coworkers [17]). Despite obvious limitations, the computational efficiency of the 1D model is very useful in investigating the interplay of different physical processes. Full-dimensional calculations for helium confirm conclusions drawn from the 1D model.

We prepare our systems in the excited states which have a predominantly one-electron excitation character, so that one of the two electrons is deeper bound than the other. We then perform exact numerical simulations of the nonrelativistic time-dependent Schrödinger equation (TDSE) and follow the dynamics of ionic excitations during one-photon, one-electron ionization by an attosecond XUV pulse. As a rule, the dynamics are initiated by the deeper bound electron, which is more likely to absorb the high-frequency photon. We can then look directly at the response and relaxation dynamics of the excited ionic subsystem initiated by the activation of the inner electron. The analysis is done in a time domain after the end of the laser pulse. Consequently, our conclusions about the underlying physics are gauge independent.

First, we observe two distinctly different excitation time scales. The first is associated with the shake-up, which is essentially instantaneous. The second is associated with the postionization interaction leading to the "knock-up" and "knock-down" transitions after the end of the laser pulse. These transitions are (somewhat) analogous to the two-step-one (TS1) process in double photoionization [18] and involve an energy exchange between the two electrons after the absorption of the XUV photon. The plausibility of different time scales for the shake-up and the knock-up transitions has been pointed out by Kheifets [19].

Second, we show that the time scales of the knock-up and knock-down transitions are directly linked to the time it takes the "active" electron, lifted from the deeper lying orbital by photon absorption, to traverse the cloud of the "passive" electron residing on the outer orbit. We show that the temporal structure of the transitions maps the space-dependent charge density of the passive electron orbitals. Depending on the initial state of the passive electron and the energy of the active electron, the relevant time scales can easily approach 10^2 asec. Thus our fully quantum analysis reveals the simple underlying semiclassical picture.

Third, we find that different time scales of the shake-up and the knock-up or knock down transitions lead to the appearance of excitation cascades. The initial shake-up excitation is followed by one or more transitions between the excited states after the end of the ionizing pulse, as the passive electron is pushed by the active one. Thus, the time-domain approach helps one to assess the physical reality of the processes described by different diagrams in the many-body perturbation theory.

For the 1D-He atom [17], the Coulomb interaction is softened by the parameters a and b (atomic units are used throughout), yielding the field-free Hamiltonian

$$\hat{H}_0 = \sum_{i=1}^{2}\left[\frac{\hat{p}_i^2}{2} - \frac{2}{\sqrt{z_i^2 + a^2}}\right] + \frac{1}{\sqrt{(z_1 - z_2)^2 + b^2}} \quad (1)$$

 ©2012 American Physical Society

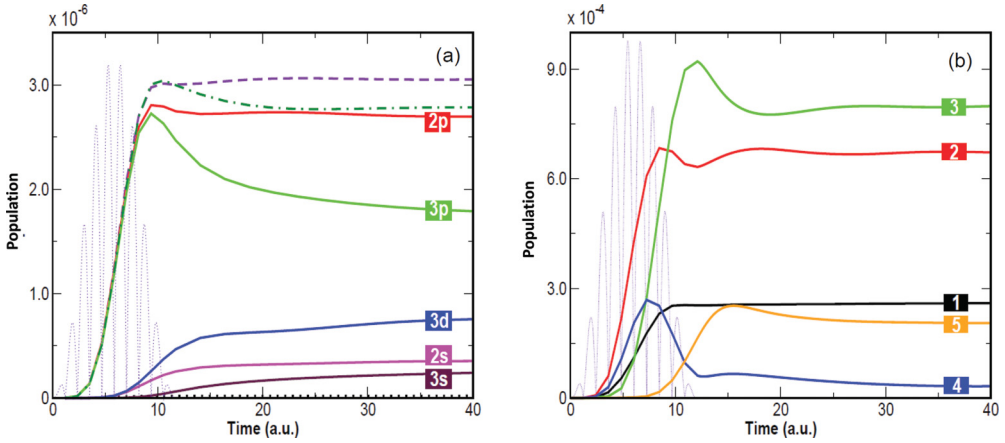

FIG. 1. (Color online) Time-dependent populations of ionic states (channels) for the 3D He (a) initially in the $1s2p\,^1P$ state and (b) the model system initially in the first excited state. The lines are marked with the corresponding channel numbers. Additionally, in panel (a) the dotted, dashed and dot-dashed lines show the cumulative populations of the ionic states with principal quantum numbers 1, 2, and 3. The populations are shown at times $A_L(t) = 0$. The fine dotted line represents $|A_L(t)|$ in arbitary units.

with the screening parameters $a = b = 0.8$. For the real three-dimensional (3D) He atom $\hat{H}_0$ is standard. We study singlet configurations, hence the spatial part of the full wave function is symmetric with respect to the exchange $\mathbf{r}_1 \Leftrightarrow \mathbf{r}_2$, $z_1 \Leftrightarrow z_2$. This symmetry is preserved during the propagation.

In both 1D and 3D calculations, the radiation field is polarized linearly along the laboratory z axis and is taken in the length gauge $V_L = (z_1 + z_2)F_L(t)$. The electric field strength of the laser pulse $F_L(t)$ is defined via the field vector potential $F_L(t) = -\dot{A}_L(t)$. The laser pulse is $A_L(t) = A_0 \sin^2(\pi t/T)\sin(\Omega t)$ with a base-to-base pulse duration $T = 2\pi N/\Omega$ where N is the number of cycles. We use $N = 2,5,10,20$ cycles in our calculations. We show results for $N = 5$ cycles, which offer a good balance of time resolution and pulse bandwidth. The carrier frequency and the peak intensity are taken $\Omega = 2.68$ a.u. and 10^{12} W/cm^2 in the full calculation and $\Omega = 2.6$ a.u. and 4×10^{15} W/cm^2 in the model. The contributions of multiphoton processes to the one-electron ionization channel remain negligible even at high intensities due to high carrier frequency.

For the 1D model, the TDSE is solved on the grid with spacing $\Delta z = 0.2$ sufficient for convergence and spanning from -200 to $+200$ in each dimension. The propagation uses the solver based on the multiconfiguration time-dependent Hartree (see [20] and the references therein) expansion of the fully symmetrized initial wave function. The implementation of the method for strong field phenomena has been described previously [21]. For the 3D calculation, we solve the two-electron TDSE using the time-dependent close-coupling method [22–24]. It is important to include a sufficient number of angular momenta l of each electron since we are interested in processes induced by the electron-electron correlation. We have carefully monitored the convergence of the solution with respect to the maximum value of l and found that $l_{\max} = 5$ is sufficient.

The initial conditions are varied in the 1D model: We start with the first and second excited states of the neutral. For the full calculation, we use the first excited $1s2p\,^1P$ state, numerically prepared through propagation in imaginary time.

To analyze the physics, we start with the 1D model. Since we are interested in the one-electron continuum, we have to project out all bound states of the neutral from the exact two-electron wave function $\Psi(z_1,z_2,t)$. Removing the bound states of the neutral that lie below the first ionization threshold (stable states) leads to

$$\Psi_I(z_1,z_2,t) = \Psi(z_1,z_2,t) - \sum_m \alpha_m(t)\psi_m(z_1,z_2)\ , \qquad (2)$$

with $\alpha_m(t) = \langle\psi_m(z_1,z_2)\,|\,\Psi(z_1,z_2,t)\rangle$, where $\psi_m(z_1,z_2)$ are the field-free bound states of the neutral. The first 20 states are sufficient to reach convergence. Next, bound states that lie above the first ionization threshold (autoionizing states) are removed. The choice of the carrier frequency and pulse duration ensures negligible population of the autoionizing states, as confirmed by projecting out all possible Hartree configurations built from the first 40 ionic (field-free) eigenstates. After the end of the laser pulse $\Psi_I(z_1,z_2,t)$ represents the "ionized" wave function with high accuracy.

Once the ionized wave function is extracted, we use it to build the wave function describing single ionization in the ionization channel i as

$$\Phi_i(z_1,z_2,t) = \chi_i^{(c)}(z_1,t)\varphi_i(z_2) + \varphi_i(z_1)\chi_i^{(c)}(z_2,t)\ , \qquad (3)$$

where $\chi_i^{(c)}(z_1,t) = \langle\varphi_i(z_2)\,|\,\Psi_I(z_1,z_2,t)\rangle$ is the continuum wave function correlated to the ionic state φ_i (the continuum wave packet in the ionization channel i). The time-dependent population of the ionic channel i is given by the norm of Φ_i.

The populations for the lower ionic channels with the neutral being initially in the first and second excited states, for the 1D model, are shown correspondingly in Figs. 1(b) and 2(a). In all cases we observe large populations of excited ionic states. Due to high photon energy, the inner electron is ejected first. If the neutral was prepared in the first excited state [Fig. 1(b)] the instant removal of the inner electron would lead to the predominant population of the first excited state of the ion (state $i = 2$) and the states of the same symmetry ($i = 4,6$, etc.). Nevertheless, we observe a large population created in the ionic state $i = 3$ (as well as in the states $i = 1,5$)

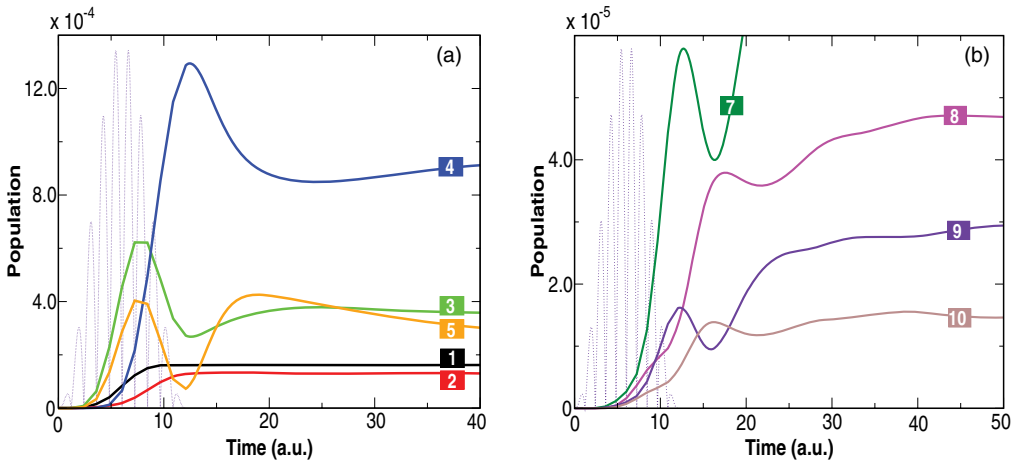

FIG. 2. (Color online) (a) Time-dependent populations of ionic states (channels) for the model system initially in the second excited state. Populations for (a) ionic channels $i = 1$–5 and (b) for ionic channels $i = 7$–10. The lines are marked with the corresponding channel numbers. The populations are shown at times $A_L(t) = 0$.

that grows during the ionizing pulse [Fig. 1(b)]. The effect is more pronounced when we prepare the neutral in the second excited state [Fig. 2(a)]. In this case the shake-up is expected to populate mostly $i = 1,3,5$, but we find that the ionic channel $i = 4$ is most important. Thus, the shake-up alone does not describe the system dynamics during the laser pulse. Moreover, the shake-up and the shake-down processes stop at the end of the pulse, around $\sim$12 a.u., while the ionic transitions continue much longer. The time scale of the postionization interaction reaches hundreds of attoseconds for our system. We refer to these delayed excitations as the knock-up process (excitation via postionization interaction between the continuum and the ionic electrons). Hence, populations of higher ionic states result from both the shake-up and knock-up processes during the laser pulse ($t \lesssim 12$ a.u.), followed by the knock-up process after the end of the laser pulse.

Similar dynamics is seen for the full-dimensional simulations [Fig. 1(a)]. Ionization of the inner electron in the $1s2p\ ^1P$ state leads to the population of the $2p$ and $3p$ states of He^+ by the shake-up process. The population changes after the end of the laser pulse correspond mainly to the $2p \to 2s$ and $3p \to (3s,3d)$ transitions, although excitations from $3p$ state to the states with higher ($\geqslant 4$) principal quantum numbers are also present. The ionic channels $2s,3s,3d$ are populated via the knock-up (correlation-driven) process. The long life of the $3p \to (3s,3d)$ transitions is caused by the slow component of the continuum electron wave packet and low transition energies. For the case of transitions between the states with the same principal quantum number, the degeneracy of the ionic states of He^+ further enhances the role of electron-electron correlation compared to other atoms without such degeneracy. We note, that both for 3D and model 1D systems, the knock-up excitation may liberate the ionic electron, and thus lead to the double ionization of the system. This channel is also open due to high photon energy, but under the conditions studied here it has a lower probability than single ionization and is not discussed in this work.

We will now analyze the physics of these delayed transitions in more detail. The only appreciable mechanism of populating the states Φ_i after the end of the laser pulse is the interaction between the continuum and the ionic electron (i.e., coupling with other Φ_j states). Other mechanisms, such as the decay of autoionizing states or population via the two-electron continuum (recapture of one of the electrons into a higher orbital) are negligible. We extend our analysis to higher ionic channels, which have a larger orbital radius and display well pronounced temporal dynamics after the laser pulse. Figure 2(b) shows time-dependent populations of higher ionic states $i = 7$–10, again for the neutral prepared in the second excited state. First, we note that the population changes in Fig. 2(b) are delayed compared to those between lower excited states [Figs. 1(b) and 2(a)]. To quantify this picture, we focus on the state $i = 8$. Using the wave function decomposed into different ionization channels in Eq. (3), we compute the time-dependent transition matrix element between the two singly ionized states, induced by the electron-electron interaction $T_{ij}(t) = \langle \tilde{\Phi}_i(z_1,z_2,t) | 1/\sqrt{(z_1 - z_2)^2 + b^2} | \tilde{\Phi}_j(z_1,z_2,t) \rangle$, where $\tilde{\Phi}_i(z_1,z_2,t)$ is the normalized to the unity singly ionized state $\Phi_i(z_1,z_2,t)$ defined in Eq. (3). This matrix element can be split into the direct and exchange parts, and we find that the direct term plays the dominant role, $T_{ij}^{(\mathrm{dir})}(t) = 2\langle \tilde{\chi}_i^{(c)}(z_1,t) | V_{ij}(z_1) | \tilde{\chi}_j^{(c)}(z_1,t) \rangle$, where $V_{ij}(z_1) = \langle \varphi_i(z_2) | 1/\sqrt{(z_1 - z_2)^2 + b^2} | \varphi_j(z_2) \rangle$ and $\tilde{\chi}_i^{(c)}(z,t)$ represents the normalized to unity wave function $\chi_i^{(c)}(z,t)$. The squared modulus of the matrix elements is shown in Fig. 3(a). In agreement with our picture, the dipole-allowed transition $7 \leftrightarrow 8$ has an earlier maximum then the dipole-allowed transition $8 \leftrightarrow 9$. The progressively increasing delays indeed reflect the larger radii of the excited states involved. Figure 3(a) demonstrates the cascade nature of the delayed transitions (excitation $7 \to 8$ is followed by the excitation $8 \to 9$).

Figure 3(b) shows that the time dependence of the matrix elements does indeed map the structure of the potentials $V_{ij}(z)$, also explaining the complex temporal profile of the quadrupole transitions $6 \leftrightarrow 8$ and $8 \leftrightarrow 10$ in Fig. 3(a). The time-space analysis of the correlated continuum wave packets $\chi_i^{(c)}(z,t)$ shows that the maxima or minima in the transition strengths

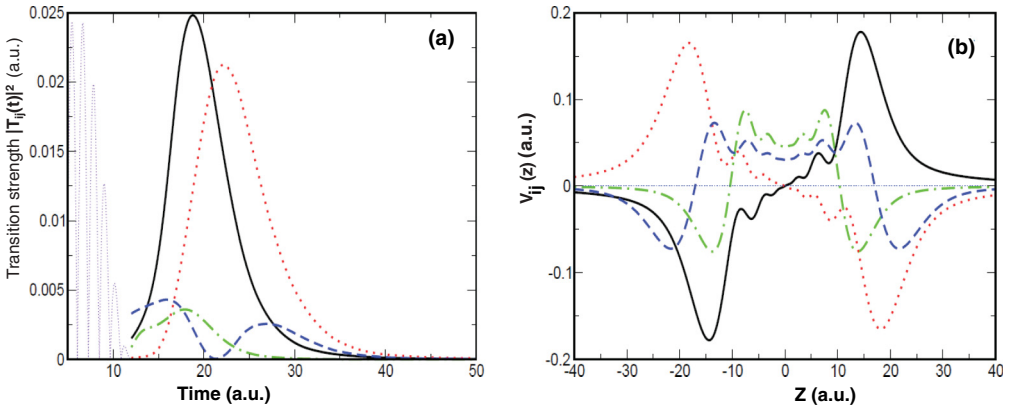

FIG. 3. (Color online) (a) Time-dependent transition strengths $|T_{ij}(t)|^2$ and (b) potentials $V_{ij}(z)$ for $i, j = 7,8$ (solid line), 8,9 (dotted line), 6,8 (dot-dashed line), and 8,10 (dashed line). Fine dotted line represents $|A_L(t)|$ in arbitrary units.

$|T_{ij}(t)|^2$ [Fig. 3(a)] occur at the times when the continuum wave packets pass through the regions where $V_{ij}(z)$ has extrema.

Thus, we confirm that the motion of the continuum electron through the electronic cloud of the bound ionic states induces a transition cascade between progressively higher-lying ionic states. The time scale of these transitions is determined by the size of the ionic states and the velocity of the continuum electron. This simple picture of the relevant time scales is very much reminiscent of attosecond temporal dynamics during multiple ionization induced by one-photon absorption, studied classically in Refs. [25,26].

The temporal picture of the electron-electron interaction dynamics which we have established suggests a pump-probe setup for resolving and controlling this two-electron dynamics. The pump pulse prepares an electronic wave packet in the superposition of the excited states of the neutral, with a predominantly one-electron character. The probe pulse, which follows the pump pulse with a delay, "activates" the inner electron by quickly promoting it to the continuum, while the outer electronic wave packet initially acts as a spectator. The pump-probe delay will control where the activated inner electron will encounter the "spectator" electron as it moves to the detector. If the outer electronic wave packet is encountered close to the core, the correlation-driven excitations will happen earlier, damping the spectator electron on the lower orbits. If the activated inner electron meets the outer electronic wave packet far from the core, the electron-electron interaction will happen later and should result in a different excitation pattern left in the ion, predominantly populating higher-lying excited states. Thus, the outer electron will work like a clock probing the motion of the second electron, with the delay-dependent excitation pattern left in the ion encoding the electron-electron interaction.

To demonstrate this effect, we prepare our model neutral atom in a superposition of the first and third excited states ($n = 2,4$), with equal weights. Both states are dominated by a single-electron excitation character. Their energy spacing of 0.152 Hartree leads to the "breathing" of the total density with a period of 41.4 a.u $\simeq$ 1 fsec. This breathing of the excited electron density is illustrated in Fig. 4(a) by projecting the total two-electron wave function onto the ionic ground state $\varphi_1(x_1)$, which approximates the state of the inner electron. Once promoted to the continuum, the inner electron will see the outer electron density, moving through it on the way to the detector. The characteristic time for the activated continuum electron to move through the cloud of the spectator electron is a few atomic units of time, much shorter than the breathing period of 41.4 a.u.

We now apply an ionizing XUV pulse as a probe and vary the time delay τ relative to $t = 0$ at which the initial wave packet is prepared. The probe carrier frequency is 2.5 a.u., the duration is five cycles base-to-base (12.57 a.u.) and the peak intensity $I = 4 \times 10^{15}$ W/cm^2. We vary the delay of the peak of the probe pulse from 7 to 70 a.u., with an increment of 1 a.u. For each peak position (τ) we propagate the Schrödinger equation for a sufficiently long time until the populations of the ionic states reach their final values. Figures 4(b) and (c) show the final populations of odd and even ionic channels, respectively, as a function of the delay τ.

As expected, ionic populations are periodic, with the period equal to that in Fig. 4(a). However, maxima and minima in each ionization channel have different amplitudes and, pertinent to this discussion, correspond to different time delays τ. To understand the physics revealed by this time delay, consider first the odd channels shown in Fig. 4(b). Due to the symmetry of the initial wave packet, only even ionic channels are populated by the shake-up mechanism [i.e., the densities shown in Fig. 4(a) represent a superposition of even ionic states only]. Odd channels are populated by the knock-up and knock-down mechanisms. According to the physical picture described above in the paper, the ionic channel i is mainly populated when the density of the outer (spectator) electron overlaps with the spatial region of the state i [more precisely, with the correlation potentials $V_{ij}(x)$ corresponding to the particular ionic orbit i]. For the ground state of the ion $i = 1$, the maximum overlap is achieved when the spectator electron is at the inner turning point of its motion (e.g., at $\tau = 41.4$ a.u.). This is, indeed, the time at which the knock-down probability to this state is maximized in Fig. 4(b). The same physical picture explains why the knock-up probability to the excited state $i = 5$ is maximized around $\tau = 20.7, 62.1$ a.u., when the spectator electron is at the outer turning point and its overlap with the ionic state $i = 5$ is maximized.

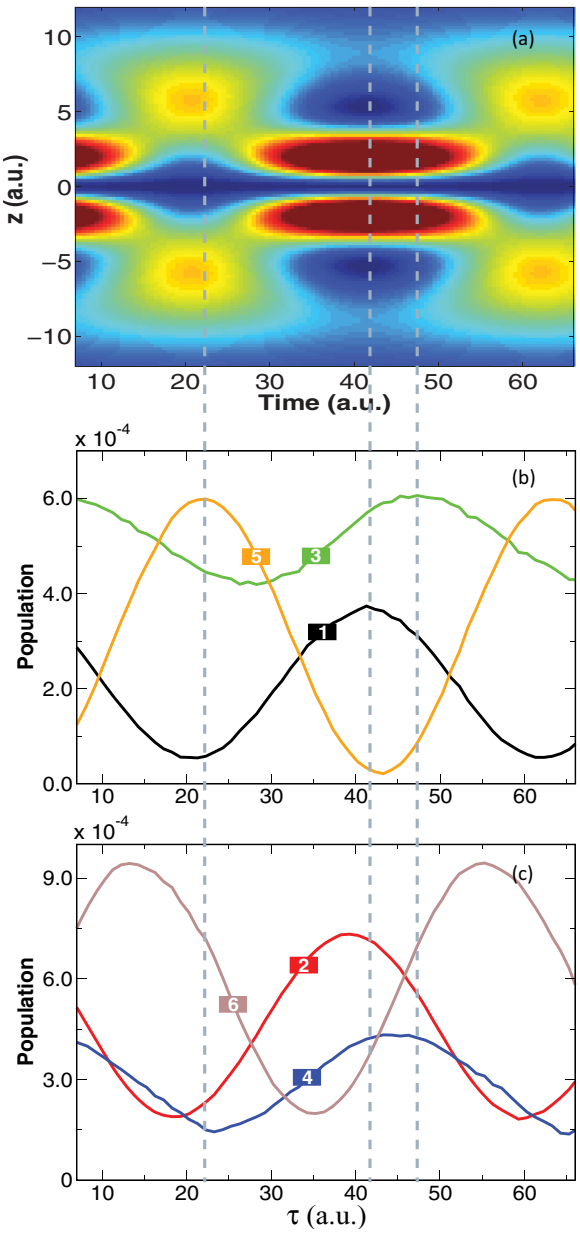

FIG. 4. (Color online) (a) Dependence of the outer electron density on time, for a superposition of the first and third excited states of the 1D Helium model. (b, c) Population of (b) odd and (c) even ionic channels as a function of the probe delay τ. Dotted lines show the maxima positions for the odd channels.

Consider now the state $i = 3$. The overlap between the spectator electron and the state $i = 3$ is maximized twice during the breathing period, just before and after the turning point, when the spectator electron is moving either away or towards the inner turning point. The first time corresponds to copropagating electrons, the second to counterpropagating. Maximum population is achieved in the case of copropagating electrons, having larger interaction time.

Let us now turn to ionic channels with even i. The dynamics is more complex since these states can be populated via both the shake-up and the postionization interaction mechanisms, with different time constants. As a result, the maximum in the population of the $i = 6$ channel shows a clear time shift relative to the $i = 5$ channel, by about 9 a.u. to earlier times. A similar shift (about 2 a.u.) is seen between the channels $i = 2$ and $i = 1$. To analyze the physics exhibited by this shift, we note that the shake-up population of $i = 2$ and $i = 6$ is predominantly created by only one neutral state among the excited pair of $n = 2,4$. In the case of the $i = 2$ state, this is $n = 2$. In the case of $i = 6$, this is $n = 4$. Thus, if only shake-up were present in the dynamics, the population of the $i = 2,6$ channels would have been almost independent of τ. The observed dependence on the delay τ in Fig. 4(c) can be explained by taking into account the postionization knock-up or knock-down transitions. The shift of the maximum in the $i = 6$ channel population towards earlier times is a result of the loss of the shake-up population via the knock-up or knock-down transitions to the neighboring states (mainly $i = 5,7$) in the vicinity of the outer turning point. The interpretation of the delay for the ionic channel $i = 2$ relative to channel $i = 1$ is analogous.

Thus, the results in Fig. 4 both support our physical picture behind the time delays in photoionization, and also demonstrate the pump-probe scheme for detecting these time delays between the formation of different ionic states (e.g., $i = 5$ and $i = 6$ in our example) without relying on the attosecond streak-camera setup.

A similar setup is possible for the helium atom. A single-photon (pump) transforms the initial ground state into the superposition of excited states $1s2p\,^1P, 1s3p\,^1P, 1s4p\,^1P, \ldots$ ($s \rightarrow p$ transition). The ionization of the system by a high-frequency photon (probe) instantly populates, by shake-up, the ionic channels $2p,3p,4p, \ldots$, while the slower knock-up and knock-down redistribute the population among all, including the missing, states. The pump-probe dependence of the population of the missing channels $1s,2s,3s,3d,4s,4d,4f, \ldots$, can then be used to resolve the correlation-driven two-electron dynamics upon the absorption of the probe photon.

Finally, we note that the postionization effect we have studied will also be well pronounced in molecules. Our study on a 1D two-electron diatom, with the internuclear distance fixed at $R = 3.0$ a.u., has shown no significant changes from the atomic case. Generally, knock-up or knock-down transitions depend on the differences in the ionic bound energies, meaning that they will be much more pronounced in large molecular systems.

M.I. thanks A. Kheifets for many stimulating and insightful discussions. This research was supported in part by the EPSRC Programme Grant No. EP/I032517/1, the Marie Curie ITN Network CORINF. We acknowledge the stimulating atmosphere of the KITPC workshop "Attosecond Science, Exploring and Controlling Matter on Its Natural Time Scale" in Beijing, and the Project of Knowledge Innovation Program (PKIP) of Chinese Academy of Sciences, Grant No. KJCX2.YW.W10. We also acknowledge the contribution of O. Smirnova who suggested the pump-probe scheme for time and space gating of the electron-electron interaction. K.L.I. gratefully acknowledges support by the APSA project (Japan) and KAKENHI (23656043 and 23104708).

[1] A. L. Cavalieri *et al*., Nature (London) **449**, 1029 (2007).
[2] P. Eckle *et al*., Science **322**, 1525 (2008).
[3] M. Schultze *et al*., Science **328**, 1658 (2010).
[4] K. Klunder *et al*., Phys. Rev. Lett. **106**, 143002 (2011).
[5] A. S. Kheifets and I. A. Ivanov, Phys. Rev. Lett. **105**, 233002 (2010).
[6] S. Nagele *et al*., J. Phys. B: At. Mol. Opt. Phys. **44**, 081001 (2011).
[7] C.-H. Zhang and U. Thumm, Phys. Rev. A **82**, 043405 (2010).
[8] J. C. Baggesen and L. B. Madsen, Phys. Rev. Lett. **104**, 209903(E) (2010).
[9] M. Ivanov and O. Smirnova, Phys. Rev. Lett., **107**, 213605 (2011).
[10] L. R. Moore, M. A. Lysaght, J. S. Parker, H. W. van der Hart, and K. T. Taylor, Phys. Rev. A **84**, 061404 (2011).
[11] J. Itatani, F. Quere, G. L. Yudin, M. Y. Ivanov, F. Krausz, and P. B. Corkum, Phys. Rev. Lett. **88**, 173903 (2002).
[12] M. Hentschel *et al*., Nature **414**, 511 (2001).
[13] P. M. Paul *et al*., Science **292**, 1689 (2001).
[14] Z. Walters and O. Smirnova, J. Phys. B **43**, 161002 (2010).
[15] A. N. Pfeiffer *et al*., Nat. Phys. **7**, 428 (2011).
[16] A. N. Pfeiffer, New J. Phys. **13**, 093008 (2011).
[17] Q. C. Su and J. H. Eberly, Phys. Rev. A **44**, 5997 (1991); see also J. Javanainen and J. H. Eberly, J. Phys. B **21**, L93 (1988); J. H. Eberly and J. Javanainen, Phys. Rev. Lett. **60**, 1346 (1988); J. Javanainen, J. H. Eberly, and Q. C. Su, Phys. Rev. A **38**, 3430 (1988).
[18] K. I. Hino, T. Ishihara, F. Shimizu, N. Toshima, and J. H. McGuire, Phys. Rev. A **48**, 1271 (1993).
[19] A. Kheifets (private communication); see also A. S. Kheifets, I. A. Ivanov and Igor Bray, J. Phys. B **44**, 101003 (2011).
[20] M. Beck, A. Jäckle, G. Worth, and H.-D. Meyer, Phys. Rep. **324**, 1 (2000).
[21] S. Sukiasyan, C. McDonald, C. Destefani, M. Y. Ivanov, and T. Brabec, Phys. Rev. Lett. **102**, 223002 (2009); S. Sukiasyan, C. McDonald, C. Van Vlack, C. Destefani, T. Fennel, M. Ivanov, and T. Brabec, Phys. Rev. A **80**, 013412 (2009); S. Sukiasyan, S. Patchkovskii, O. Smirnova, T. Brabec, and M. Y. Ivanov, *ibid.* **82**, 043414 (2010).
[22] K. L. Ishikawa and K. Midorikawa, Phys. Rev. A **72**, 013407 (2005).
[23] J. S. Parker, L. R. Moore, K. J. Meharg, D. Dundas, and K. T. Taylor, J. Phys. B **34**, L69 (2001).
[24] M. S. Pindzola and F. Robicheaux, Phys. Rev. A **57**, 318 (1998); J. Phys. B **31**, L823 (1998); J. Colgan, M. S. Pindzola, and F. Robicheaux, *ibid*. **34**, L457 (2001).
[25] A. Emmanouilidou and J. M Rost, Phys. Rev. A **75**, 022712 (2007).
[26] A. Emmanouilidou, P. Wang, and J. M. Rost, Phys. Rev. Lett. **100**, 063002 (2008).